

# Technical aspects of MR diffusion imaging of the body

Olaf Dietrich<sup>1</sup>, Andreas Biffar<sup>1</sup>, Andrea Baur-Melnyk<sup>2</sup>, Maximilian F. Reiser<sup>1,2</sup>

<sup>1</sup> Josef Lissner Laboratory for Biomedical Imaging, Department of Clinical Radiology – Grosshadern, LMU Ludwig Maximilian University of Munich, Munich, Germany

<sup>2</sup> Department of Clinical Radiology – Grosshadern, LMU Ludwig Maximilian University of Munich, Munich, Germany

## ELECTRONIC PREPRINT VERSION:

*Not for commercial purposes or for any external distribution by a third party.*

## Abstract:

In diffusion-weighted magnetic resonance imaging (DWI), the intensity of the acquired magnetic resonance signal depends on the self-diffusion of the excited spins, i. e., on the microscopic stochastic Brownian molecular motion. Since the extent and orientation of molecular motion is influenced by the microscopic structure and organization of biological tissues, DWI can depict various pathological changes of organs or tissues.

While DWI of the brain can be considered an established technique since the mid-1990s, significantly fewer studies have been published about DWI in body imaging, mainly because of the relatively low robustness of conventional DWI methods in non-neurological applications. Consequently, the image quality in such applications was rather limited. This situation, however, improved considerably in recent years due to better hardware as well as new pulse sequences, and several new applications of DWI (e. g., in the abdominal organs, in musculoskeletal applications, or in whole-body protocols) have been described.

Unfortunately, DWI of the body is complicated by frequently low signal-to-noise ratios due to shorter transversal (T2) relaxation times and by strong variations of susceptibility. The latter result in severe distortion artifacts when standard echo-planar DWI techniques are applied. Hence, several alternative (non-echo-planar) dif-

fusion-weighting pulse sequence types were proposed and evaluated for DWI applications in the body.

In this review article, first the basics of molecular diffusion and of diffusion-weighted MRI are introduced and then several specific MRI techniques, which have been used for DWI of the body, are described. Finally, protocol recommendations for different DWI applications in the body are provided.

### *Key words:*

Diffusion-weighted magnetic resonance imaging; Pulse sequences; Image artifacts; Protocol recommendations

### *Corresponding author:*

Olaf Dietrich, PhD  
Josef Lissner Laboratory for Biomedical Imaging  
Department of Clinical Radiology – Grosshadern  
LMU Ludwig Maximilian University of Munich  
Marchioninstr. 15  
81377 Munich  
Germany  
Phone: +49 89 7095-4622  
Fax: +49 89 7095-4627  
E-mail: [od@dtrx.net](mailto:od@dtrx.net)

## Introduction

In diffusion-weighted magnetic resonance imaging (DWI), the intensity of the acquired magnetic resonance signal depends on the self-diffusion of the excited spins, i. e., on the microscopic stochastic Brownian (or thermal) molecular motion. Since the extent and orientation of molecular motion is influenced by the microscopic structure and organization of biological tissues, DWI can depict various pathological changes of organs or tissues. Numerous studies evaluated DWI for the assessment of neurological pathologies<sup>1</sup> and in particular for the early detection of cerebral ischemia<sup>2,3</sup>, which is generally considered the most important clinical application of DWI.

While DWI of the brain can be considered an established technique since the mid-1990s, significantly fewer studies have been published about DWI in body imaging, mainly because of the relatively low robustness of conventional DWI methods in non-neurological applications. Consequently, the image quality in such applications was rather limited. This situation, however, improved considerably in recent years due to better hardware as well as new pulse sequences, and several new applications of DWI have been described. Examples are DWI studies of the liver<sup>4-6</sup>, the kidneys<sup>7-9</sup>, the breast<sup>10-13</sup>, the prostate<sup>14-16</sup>, and the lymph nodes<sup>17,18</sup>, as well as of the musculoskeletal system including the assessment of soft-tissue tumors<sup>19,20</sup> and in particular of benign and malignant vertebral compression fractures<sup>21-23</sup>. Recently, whole-body DWI was proposed to improve the detection and characterization of malignancies<sup>24,25</sup>.

Unfortunately, DWI of the body is complicated by the frequently low signal-to-noise ratio (SNR) due to shorter transversal (T2) relaxation times and by significantly stronger variations of susceptibility than, e. g., in the brain. The latter result in severe distortion artifacts when standard echo-planar DWI techniques are applied<sup>26,27</sup>; particularly, at higher field strengths of 3 Tesla or more<sup>28</sup>. Hence, several alternative diffusion-weighting pulse sequence types were proposed and evaluated for DWI of the body as described below.

In this review article, we first introduce the basics of diffusion and diffusion-weighted MRI and

then describe several specific MRI techniques, which have been used for DWI of the body. Finally, we will provide general protocol recommendations for different DWI applications in the body.

## Basics of diffusion and diffusion-weighted MRI

### Physical background

DWI is a magnetic resonance (MR) technique that is sensitive to the Brownian molecular motion of spins<sup>29</sup>. The molecular motion (diffusion) is related to the thermal kinetic energy,  $E_{kin}$ , of the molecules, which is proportional to the temperature,  $T$ :

$E_{kin} = \frac{3}{2} k_B T$ ; here,  $k_B = 1.38 \times 10^{-23}$  J/K is the Boltzmann constant. Higher thermal energies are associated with faster molecular motion; the average velocity,  $v$ , of a free (gas) molecule with energy  $E_{kin}$  is  $v = \sqrt{2E_{kin}/m} = \sqrt{3k_B T/m}$ . The thermal molecular motion is completely stochastic and in many cases, e. g. in gases or liquids, isotropic; it should not be confused with flow or other directed processes. In particular, diffusion only increases the standard deviation of the position of a molecule but not its mean position as illustrated in Fig. 1.

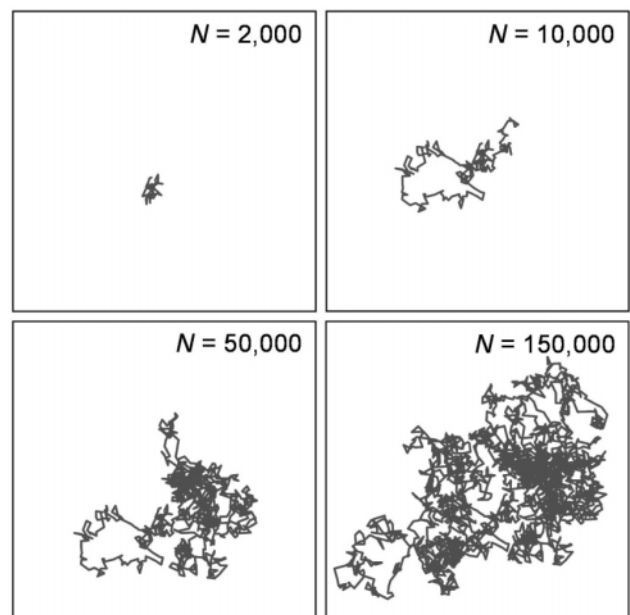


**Figure 1:** Simulated isotropic diffusion path of a single molecule; random-walk simulation after  $N = 2000$ , 10 000, 50 000, and 150 000 simulated steps. The simulations demonstrate that the mean value of the position remains at the origin (at the center of the plots), while the standard deviation increases proportional to the square root of the diffusion time (corresponding to the number,  $N$ , of simulated steps).

**Table 1:** Examples of diffusion coefficients of water and different biological tissues

	ADC ( $10^{-3}$ mm <sup>2</sup> /s)
Water, 20 °C <sup>77</sup>	2.02
Water, 35 °C <sup>78</sup>	2.92
Brain, white matter <sup>79</sup>	0.70
Brain, gray matter <sup>79</sup>	0.89
Liver <sup>4</sup>	1.83
Kidney (cortex) <sup>8</sup>	2.43
Kidney (medulla) <sup>8</sup>	2.16
Breast (fibroglandular tissue) <sup>10</sup>	2.37
Prostate (peripheral zone) <sup>14</sup>	1.95
Prostate (central gland) <sup>14</sup>	1.53
Vertebral bone marrow <sup>23</sup>	0.2 – 0.5

The diffusion of molecules in a liquid or in a gas is quantitatively described by the diffusion coefficient,  $D$ . The diffusion coefficient is frequently given in units of mm<sup>2</sup>/s and describes the mean displacement,  $d$ , i. e., the mean diameter of the three-dimensional extension (or, more exactly, the standard deviation of the position  $\sqrt{\langle \mathbf{x}^2 \rangle}$ ) of the stochastic molecular motion within a time, (usually referred to as diffusion time):

$$d = \sqrt{\langle \mathbf{x}^2 \rangle} = \sqrt{6 \cdot D \cdot \tau}.$$

The diffusion coefficient of pure water at room temperature, for instance, is approximately  $2 \times 10^{-3}$  mm<sup>2</sup>/s, resulting in a mean displacement of about  $d = 25$  μm in a diffusion time of 50 ms. More examples of diffusion coefficients in different biological tissues are presented in Table 1.

### Diffusion-sensitized MRI

Already in 1950, Erwin Hahn described that the presence of a magnetic field gradient during a magnetic resonance spin-echo experiment results in a signal attenuation due to the molecular diffusion of the spins<sup>30</sup>. An improved strategy to quantify the diffusion coefficient,  $D$ , in a magnetic resonance experiment was proposed in 1965 by Stejskal and Tanner<sup>31</sup>. In their experiment, a pair of additional gradient pulses was inserted into a pulse

sequence, the so-called Stejskal-Tanner diffusion gradients. This technique (sometimes slightly modified) is still in use today in the majority of all diffusion-weighting sequences.

The effect of these diffusion gradients is to attenuate the transversal magnetization, i. e., the received MR signal intensity, depending on the extent of molecular motion as illustrated in Fig. 2. This attenuation effect is based on the proportionality of the Larmor or precession frequency,  $\omega_L$ , of a spin and the external magnetic field,  $B$ :  $\omega_L = \gamma \cdot B$ , where the proportionality factor  $\gamma$  is called the "gyromagnetic ratio"; in the case of normal proton-MRI, this is  $\gamma = 267.5 \times 10^6$  rad s<sup>-1</sup> T<sup>-1</sup>. A gradient pulse with amplitude,  $g_D$ , in, e. g., x-direction causes an additional spatially linear magnetic field  $\Delta B(x) = g_D \cdot x$  and, thus, a spatially depending variation of the Larmor frequency by  $\Delta\omega_L(x) = \gamma \cdot \Delta B(x) = \gamma \cdot g_D \cdot x$ . The additional phase angle after this gradient pulse of duration,  $\delta$ , is  $\Delta\phi(x) = \Delta\omega_L(x) \cdot \delta = \gamma \cdot g_D \cdot x \cdot \delta$ , which depends linearly on the position,  $x$ , as well. Hence, spins at different positions,  $x$ , are equipped with different additional phase angles after the gradient pulse, i. e., they are "dephased" (not longer precessing with the same phase). The opposite process, i. e., returning dephased spins into states with identical phases, is called "rephasing".

Dephasing and rephasing are the mechanisms employed for diffusion weighting. The first diffusion gradient dephases the spins, i. e., the spins are prepared with a spatially varying additional phase angle,  $\Delta\phi(x)$ . Spins at the position of lower magnetic fields (left hand side in the illustration since the gradient field increases linearly from left to right) are prepared with smaller additional phase angles than spins at higher magnetic fields. In the case of stationary spins, this additional phase angle is exactly reverted by the second diffusion gradient, resulting in the same transversal magnetization after the second gradient as without diffusion sensitizing. If, however, the spins move stochastically between the two diffusion gradients, then each single spin experiences a different magnetic field at the time of the second gradient pulse, which does not compensate the effects of the first (dephasing) gradient pulse. Consequently, the second gradient does not fully revert the dephasing and a certain, stochastically distributed phase angle remains. This

random distribution of phase angles is observed as signal attenuation, which is, thus, a measure of molecular diffusion. Frequently, the diffusion gradients are positioned at both sides of a refocusing (180°) radio frequency (RF) pulse – in this case, they appear in the sequence diagram with identical polarity and the rephasing effect of the second gradient requires the phase flip caused by the 180° pulse.

The observed attenuation of the magnetic resonance signal is defined as the ratio of the measured signal,  $S(D, b)$ , and the original signal without diffusion gradients,  $S_0$ . This ratio,  $S(D, b) / S_0$ , depends exponentially on the diffusion coefficient,  $D$ , and on the properties of the diffusion gradients, which are summarized within the so-called diffu-

sion weighting,  $b$ , or b-value of the pulse sequence:

$$S(D, b) = S_0 \cdot \exp(-b \cdot D).$$

The b-value of the sequence can be calculated from the properties of the diffusion gradients shown in Fig. 2, i. e., from their amplitude,  $g_D$ , their duration,  $\delta$ , and the interval between their onsets,  $\Delta$ :

$$b = (\gamma \cdot g_D \cdot \delta)^2 \cdot (\Delta - \delta/3),$$

where  $\gamma$  is the gyromagnetic ratio of the diffusing spins. The b-value is frequently expressed in units of  $s/mm^2$ ; typical values for DWI range from 50 to 1500  $s/mm^2$  (but higher values may be used for specific applications). To obtain these b-values, relatively long and strong diffusion gradients are required; typical gradient durations are  $\delta = 20 \dots 40$  ms and typical gradient amplitudes are  $g_D = 20 \dots 40$  mT/m.

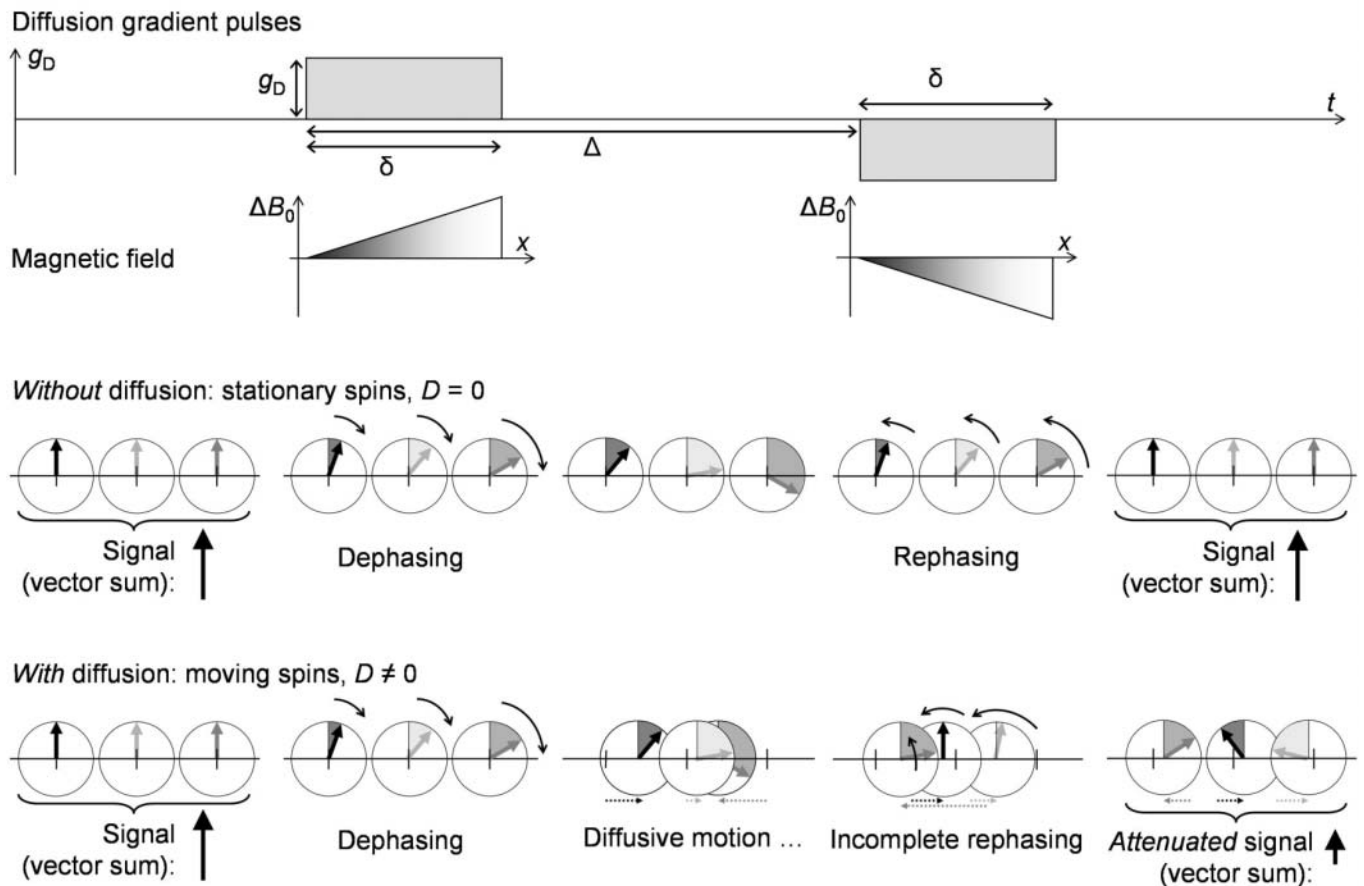


**Figure 2:** Effect of diffusion gradients. The diffusion gradients (top row) cause a spatially varying additional magnetic field,  $\Delta B(x)$ , (second row) and, thus, spatially varying Larmor frequencies. The first diffusion gradient dephases the spins (three spins at different spatial positions are shown as grey and black arrows in a circle). If the spins are stationary (no diffusion), the second diffusion gradient with opposite sign exactly rephases the spins. In the case of diffusing spins, however, rephasing is incomplete since the spins have moved between the first and the second diffusion gradient; thus, a diffusion-dependent signal attenuation is observed as illustrated by the “vector sum” arrows.

The b-value of a pulse sequence plays the same role in DWI as the echo time in  $T_2$ -weighted MRI: Higher diffusion weightings increase exponentially the contrast between tissues with different diffusion coefficients, but at the same time they decrease the overall signal intensity. Hence, the choice of the optimal diffusion weighting (which is discussed in detail below) must always be considered as a compromise between maximizing the diffusion contrast on the one hand and the signal-to-noise ratio (SNR) on the other hand<sup>32</sup>. Obtaining a sufficient SNR is particularly demanding in DWI, since the SNR of diffusion-weighted images is additionally reduced by relatively long echo times, which are required due to the long duration,  $\delta$ , of the diffusion gradient pulses.

Another general problem of DWI is the very high motion sensitivity of diffusion-sensitized pulse sequences<sup>33-35</sup>. Since the diffusion gradients are inserted in order to depict stochastic molecular motions in the range of some 10 micrometers, DWI becomes very sensitive to any macroscopic patient motions as well. The most important sources of such motion are pulsatile blood flow, CSF pulsation, cardiac or respiratory motion, and peristaltic bowel motion. Several different approaches were suggested in order to increase the robustness of DWI techniques as described below.

### Diffusion tensor MRI

In applications of DWI in vivo, the by far most important diffusing molecule is water. Generally, water diffusion in tissue is influenced by the properties of the cells, in particular by the cell size and their geometric structure. Typical diffusion coefficients of water measured in vivo are in the range between about  $0.3$  and  $3 \times 10^{-3}$  mm<sup>2</sup>/s (the diffusion coefficient of pure water at body temperature (37 °C) is approximately  $3.1 \times 10^{-3}$  mm<sup>2</sup>/s). Thus, the observed diffusion coefficients are decreased compared to free water diffusion due to the presence of cell membranes, cell organelles, or large macromolecules, which restrict and hinder the molecular motion. The actually measured diffusion coefficient in vivo is therefore called "apparent diffusion coefficient" (ADC).

By applying diffusion gradients in a single spatial direction as illustrated in Fig. 2, only diffusional motion parallel to this direction is detected. While this experiment is sufficient to measure the diffu-

sion properties of, e. g., isotropic liquids, the situation in biological tissue can be much more complex. In particular in highly anisotropic tissues such as nerve or muscle fibers, diffusion will be lower perpendicular than parallel to the fiber direction since the distance of diffusion-hindering cell membranes will be smaller perpendicular to the fiber orientation. Thus, the diffusing molecules will be more frequently influenced by cell membranes in perpendicular direction, resulting in a decreased apparent diffusion coefficient. In this case, diffusion is not longer described by a single (scalar) diffusion coefficient but by the diffusion tensor,  $\mathbf{D}$ , which can be represented by a symmetric  $3 \times 3$  matrix containing 6 independent values<sup>36, 37</sup>:

$$\mathbf{D} = \begin{pmatrix} D_{xx} & D_{xy} & D_{xz} \\ D_{xy} & D_{yy} & D_{yz} \\ D_{xz} & D_{yz} & D_{zz} \end{pmatrix}$$

To measure the diffusion tensor, several diffusion measurements (at least 6 corresponding to the number of independent matrix components) are required, which can be obtained by applying diffusion gradients in different spatial directions<sup>38</sup>; this acquisition is known as diffusion tensor imaging (DTI).

Three important quantities that can be calculated from the diffusion tensor are the mean diffusivity, the diffusion anisotropy, and the main diffusion orientation. The mean diffusivity,  $D_{\text{mean}}$ , describes the diffusion coefficient averaged over all spatial directions; it can be calculated as a third of the trace of the diffusion tensor, i. e., of the sum of the three diagonal matrix elements,

$$D_{\text{mean}} = \frac{1}{3}(D_{xx} + D_{yy} + D_{zz}).$$

The diffusion anisotropy describes how much the diffusion deviates from isotropic (i. e., spherically symmetric) diffusion: high anisotropies correspond to diffusion processes with a strongly preferred spatial orientation. The diffusion anisotropy is frequently expressed as the fractional anisotropy, FA; to calculate the anisotropy, the matrix is first transformed into a diagonal matrix

$$\mathbf{D} = \begin{pmatrix} D_1 & 0 & 0 \\ 0 & D_2 & 0 \\ 0 & 0 & D_3 \end{pmatrix}$$

with the eigenvalues  $D_1, D_2, D_3$  and the corresponding eigenvectors  $\mathbf{v}_1, \mathbf{v}_2, \mathbf{v}_3$ . The fractional anisotropy is then given by

FA =

$$\frac{\sqrt{3}}{\sqrt{2}} \frac{\sqrt{(D_1 - D_{\text{mean}})^2 + (D_2 - D_{\text{mean}})^2 + (D_3 - D_{\text{mean}})^2}}{\sqrt{D_1^2 + D_2^2 + D_3^2}}$$

Each eigenvector  $v_1, v_2, v_3$  is associated with an eigenvalue,  $D_1, D_2, D_3$ , and the eigenvector associated with the largest eigenvalue describes the main (or principal) diffusion orientation. E. g. in nerve or muscle fibers, the main diffusion direction is parallel to the fiber orientation and can therefore be used to visualize the fiber tracts; this process is called fiber tracking or diffusion tractography<sup>39</sup>.

### Pulse sequences for DWI of the body

Many different types of pulse sequences can be modified for DWI by inserting additional diffusion-

sensitizing (Stejskal-Tanner) gradients. The most important sequences are discussed in the following sections:

#### Spin-echo and stimulated-echo sequences

Historically, DWI was first performed with stimulated-echo and spin-echo pulse sequences (Fig. 3a,b)<sup>40-42</sup>. These pulse sequences, however, require very long acquisition times of several minutes to acquire a single multi-slice data set since they fill the required raw-data space (k-space) line by line with echoes (Fig. 3e), whose acquisitions are separated by the relatively long repetition time, TR, of 2 to 5 seconds. These sequences are very prone to motion artifacts, which result from different states of involuntary patient motion in subsequently acquired k-space lines.

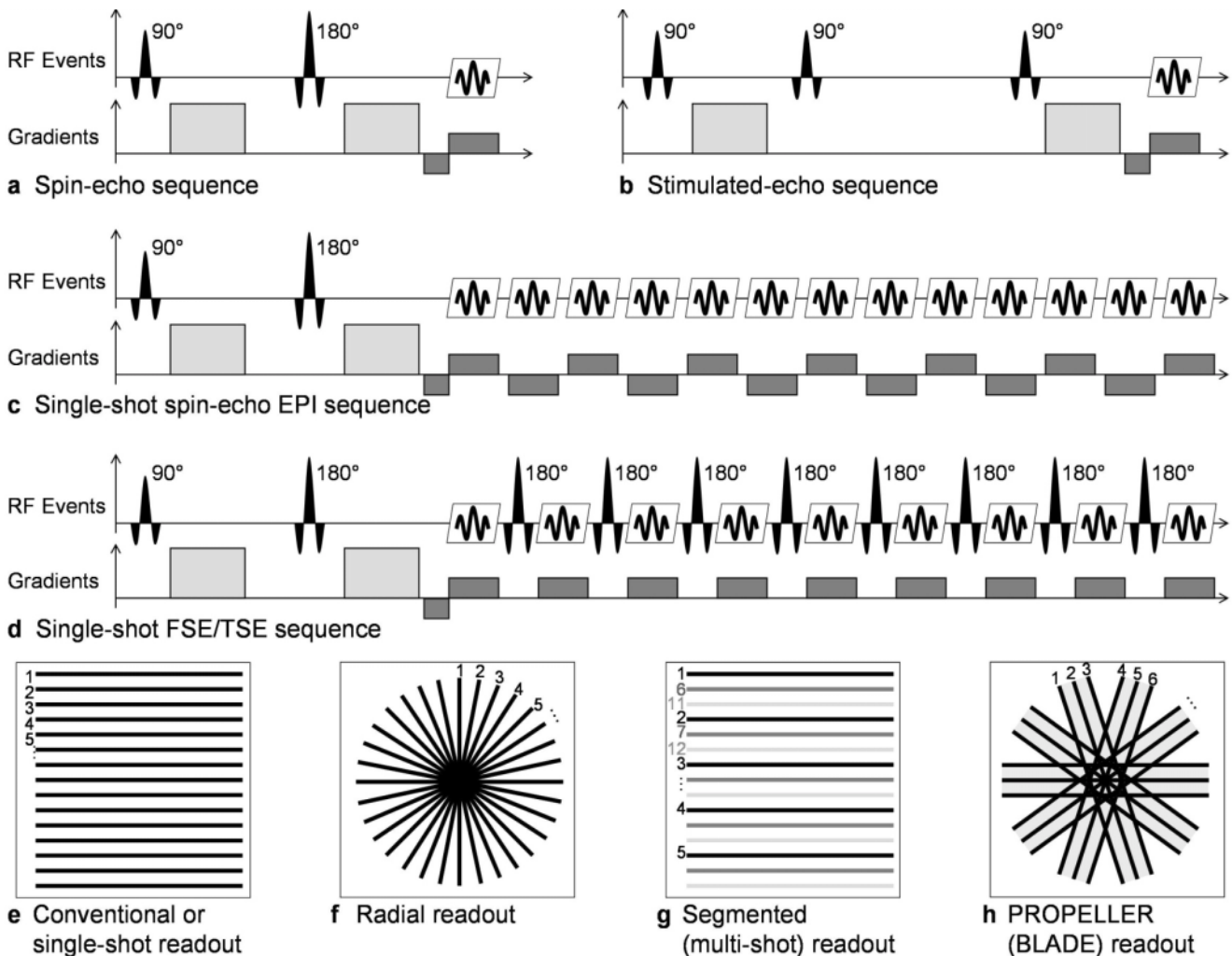


**Figure 3:** Pulse sequences used for quantitative DWI. Sequences are simplified by displaying only the diffusion gradients (light-gray boxes) and the imaging gradients in readout direction (dark-gray boxes). (a, b) a single repetition of a spin-echo and stimulated-echo sequence, and (c, d): echo trains of single-shot spin-echo echo-planar and fast-spin-echo sequences; (e-h) k-space trajectories for conventional, radial, segmented, and PROPELLER acquisitions.

Although different strategies were proposed to reduce the motion sensitivity and increase the robustness of stimulated-echo and spin-echo sequences such as navigator-echo motion correction<sup>43–45</sup> or radial k-space sampling (Fig. 3f)<sup>46,47</sup>, these sequence types are practically not used any more in clinical MRI because of their prohibitively long acquisition times. This disadvantage is overcome to a certain degree by a modification of the conventional spin-echo sequence called diffusion-weighted line-scan-imaging technique, proposed by Gudbjartsson et al. in 1996<sup>48</sup>. In line-scan imaging, only one-dimensional lines of the imaged volume are excited instead of complete two-dimensional slices. Thus, the acquisition time and the motion sensitivity can be reduced, at the cost, however, of a lower SNR. A second disadvantage is that line-scan imaging techniques are not available for all MRI systems.

### ***Echo-planar imaging (EPI) sequences***

The most important and most frequently used pulse sequence for DWI in general is the single-shot spin-echo echo-planar imaging sequence (Fig. 3c)<sup>49</sup>. This sequence is relatively insensitive to influences from macroscopic patient motion because of the very fast readout of the complete image data within about 100 ms. The fast and – with respect to motion sensitivity – relatively robust acquisition are the most important reasons that the single-shot EPI sequence became the standard technique for DWI and DTI of the brain.

In the presence of  $B_0$  inhomogeneities and susceptibility variations, however, echo-planar images frequently suffer from gross geometrical image distortions due to the relatively long gradient-echo train. Susceptibility variations translate to variations of the Larmor frequencies of spins and, thus, to phase errors in the k-space data that accumulate over the duration of the echo train<sup>26</sup>. This property of EPI is a severe limitation for the application outside the brain (where distortions are limited to few, well-known areas) and particularly for structures or organs found in the direct neighborhood of air-filled spaces (e.g., the lungs) or bone-soft-tissue interfaces with substantially different susceptibilities. A second disadvantage of single-shot EPI is the relatively low spatial resolution of typically 128×128 pixels that can be realized with

this approach due to the rapid T2\* decay of the signal during the gradient-echo train.

One approach to increase the spatial resolution and to reduce the occurrence of distortion artifacts of EPI acquisitions is a segmented (or multi-shot) echo-planar readout: The echo train of a single image can be divided in several parts that are shorter than the original single-shot readout (Fig. 3g). The total acquisition time of a slice, however, is considerably increased in multi-shot acquisitions, since the excitation pulses for each segment must be separated by a repetition time of typically a few seconds. On the one hand, by shortening the echo train length, the segmented EPI sequence becomes less sensitive to susceptibility variations, shows reduced distortion artifacts, and its spatial resolution can be easily increased. On the other hand, its robustness against motion artifacts is substantially reduced as different states of patient motion may now occur for each acquired segment. Navigator-echo correction schemes similarly as mentioned above for the spin-echo approach have been applied for segmented EPI to correct for the influences of motion<sup>50</sup>.

Only relative recent innovations in hardware and in acquisition techniques substantially improved the suitability of EPI for body DWI. Improved gradient systems with reduced eddy-current effects can decrease geometric distortions. Even more important became the application of parallel imaging techniques<sup>51</sup> such as sensitivity-encoded (SENSE) MRI<sup>52</sup> or the generalized autocalibrated partially parallel acquisition (GRAPPA) technique<sup>53</sup>. Parallel imaging can be used to reduce the echo-train length and, thus, the geometric distortions in echo-planar imaging and, at the same time, to increase the spatial resolution of EPI to 192×192 or even 256×256 pixels<sup>54</sup>.

### ***Fast-spin-echo or turbo-spin-echo sequences***

An alternative to diffusion-weighted EPI acquisitions are diffusion-weighted single-shot fast-spin-echo (or turbo-spin-echo) sequences. These sequences are also known as diffusion-weighted “rapid acquisition with relaxation enhancement” (RARE) or “half-Fourier-acquisition single-shot turbo-spin-echo” (HASTE) sequences (Fig. 3d)<sup>55, 56</sup>. Similar to echo-planar acquisition techniques, these sequences are very fast (with acquisition times in the order of 200–400 ms per image) and relatively

insensitive to motion, but provide only limited spatial resolution of typically  $128 \times 128$  pixels due to the T2 decay of the signal during the spin-echo train.

An important advantage of this sequence type particularly for non-neurological applications such as DWI of the musculoskeletal system is the insensitivity to susceptibility variations: Variations of the Larmor frequencies are inherently compensated by the refocusing RF pulses. Unfortunately, inserting diffusion gradients into the spin-echo train destroys the originally equal spacing of refocusing RF pulses (which is required for optimal signal formation and referred to as Carr-Purcell-Meiboom-Gill (CPMG) condition) and can induce new image artifacts. Several approaches have been suggested to overcome this disadvantage, but most solutions also reduce the SNR of the acquired images<sup>55, 57, 58</sup>. More recently proposed solutions can recover (almost) the full SNR<sup>59, 60</sup>, but are not yet generally available on most MRI systems. Parallel imaging can be employed to increase the spatial resolution and to reduce the typical blurring artifacts in phase-encoding direction caused by the T2 decay of the signal.

Similarly as in multi-shot EPI acquisitions, the fast-spin-echo readout can be segmented in order to increase the spatial resolution or to reduce blurring artifacts; at the cost, however, of prolonged acquisition times and higher motion sensitivity. A related and particularly promising approach is the recently proposed diffusion-weighted PROPELLER (periodically rotated overlapping parallel lines with enhanced reconstruction) or BLADE (Siemens Healthcare, Erlangen, Germany) sequence<sup>61, 62</sup>. With these segmented, non-Cartesian acquisition techniques, the k-space is covered by several rotated rectangular strips, each consisting of a fast-spin-echo train (Fig. 3h). The sequence is self-navigated since all these strips (or blades) include an area around the center of the k-space. This allows for motion correction similarly as in purely radial spin-echo techniques but with higher robustness due to the larger oversampled central k-space area.

### **Steady-state free-precession (SSFP) sequences**

Diffusion-weighted imaging with the steady-state free-precession (SSFP) sequence differs considerably from almost all other DWI approaches, which employ variants of the conventional Stejskal-Tanner

diffusion-gradient scheme. The SSFP sequence type used for DWI is the diffusion-weighted contrast-enhanced Fourier-acquired steady-state technique (CE-FAST; here, 'contrast-enhanced' refers to the inherent image contrast and not to the administration of contrast media) or PSIF sequence<sup>63, 64</sup>. The PSIF sequence is a reversed version (with respect to the timing of the pulse sequence events and also to the spelling of the acronym) of the "fast imaging with steady precession" (FISP) sequence. In contrast to the other approaches described above, only a single (monopolar) diffusion gradient is typically inserted into each repetition time, TR, of the PSIF sequence (Fig. 4a shows two subsequent TRs)<sup>65, 66</sup>.

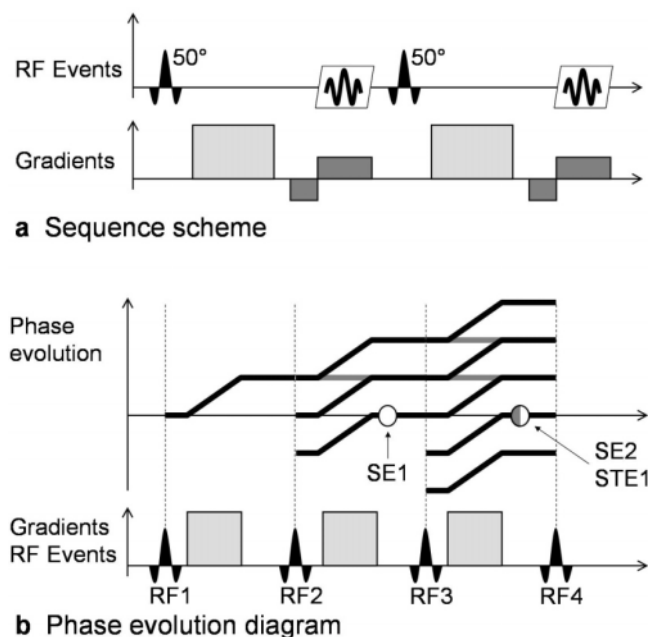


**Figure 4:** Diffusion-weighted steady-state free-precession (SSFP) pulse sequence: (a) Simplified sequence scheme with diffusion gradients (light-gray boxes) and imaging read-out gradients (dark-gray boxes); two subsequent repetitions are displayed. (b) Phase evolution diagram of the SSFP diffusion sequence; phase angles are increased by diffusion gradients and (partially) inverted by the RF pulses (see text).

Spins dephased by this diffusion gradient are rephased by a following diffusion gradient later in the sequence scheme (i. e., in one of the following repetitions); however, not necessarily by the immediately subsequent one. This can be illustrated in a phase-evolution diagram (Fig. 4b): The first diffusion gradient (light-gray box) adds an extra phase to the spins (as indicated by the first ramp in the upper part of the diagram). The second RF pulse, RF2, (with a flip angle of typically  $50^\circ$ ) partially reverts the phase, leaves other spins in their current state, and rotates a third fraction of the spins into the longitudinal direction (indicated by the gray line; these longitudinal spins are not dephased by the following diffusion gradient). Only the reverted spins form the first spin echo (SE1) after the second diffusion gradient (i. e., after a diffusion time of about  $1 \times TR$ ); the other spins remain dephased and evolve further until the next RF pulse (RF3) acts on them. Again, some spins are flipped by  $180^\circ$ , some are left unchanged, and some are moved from the longitudinal direction back into the transversal plane. This last group forms a first stimulated echo (STE1) after a diffusion time of about  $2 \times TR$ . Other spins are rephased even later. Thus, the experienced diffusion times can be very different for the spins that contribute to the observed signal. Consequently, the effective diffusion weighting,  $b$ , of the PSIF sequence cannot easily be calculated, but depends in a complicated way on the relaxation times of tissue,  $T_1$  and  $T_2$ , as well as on the sequence parameters,  $TE$ ,  $TR$ , and the flip angle<sup>67,68</sup>. Although the exact quantification of the ADC is therefore almost impossible, diffusion-weighted PSIF images have been shown to be extremely valuable for the differential diagnosis of vertebral compression fractures based on the visual (non-quantitatively evaluated) image contrast between lesions and surrounding vertebral bodies<sup>21–23</sup>.

The diffusion-weighted PSIF sequence is relatively fast due to the short repetition times in the order of typically 20 to 30 ms. Consequently, this approach is also relatively insensitive to the influence of bulk motion. Newer developments of SSFP DWI include the implementation of diffusion-weighted 3D sequences, which have been applied, e. g., for DWI of the cartilage<sup>69</sup>.

## Protocol considerations for DWI of the body

### *Sequence recommendations for DWI of the body*

In contrast to DWI of the brain, for which EPI sequences are the established and generally accepted acquisition technique, there is no such general agreement on the optimal method for DWI of the body and in particular of the musculoskeletal system. Particularly in the neighborhood of interfaces of tissues with different susceptibilities, the image quality and the reliability of the measured quantitative parameters can be very low when applying EPI sequences due to severe image distortions and artificial signal variations. Typical examples are DWI studies in the neck/shoulders region<sup>70</sup>, in the thorax, or of the spinal column. In such cases, single-shot fast-spin-echo techniques or robust segmented techniques such as PROPELLER or BLADE sequences are preferable for quantitative DWI.

On the other hand, echo-planar imaging has substantially improved in recent years due to enhanced gradient systems, better shim algorithms, and new reconstruction techniques such as parallel imaging. In the liver or the kidneys, acceptable image quality can now be obtained with diffusion-weighted EPI techniques on state-of-the-art MR systems. Generally, the length of the echo train should be minimized, e.g., by applying parallel imaging with reduction (acceleration) factors of 2 or 3 and – additionally – by partial-Fourier techniques. Due to its unsurpassed speed, there is still no established alternative to diffusion-weighted EPI when diffusion tensor data is to be acquired in clinically acceptable acquisition times. In combination with breath-hold acquisitions as required for DTI of the liver and the kidneys, only EPI provides sufficient speed in order to acquire data in a sufficient number of diffusion directions.

Special DWI applications such as the assessment of vertebral compression fractures can benefit from alternative imaging techniques and in particular from non-quantitative DWI based on SSFP techniques. The potential of this approach, e. g., for the detection of malignancies outside the musculoskeletal system, is not yet fully explored.

### The optimal diffusion weighting for DWI of the body

An important parameter for all DWI studies is the (maximal)  $b$ -value of the applied pulse sequence. On the one hand, the contrast between tissues with different ADCs increases with higher  $b$ -values. On the other hand, this process is limited by the available SNR, since the overall signal intensity decreases with increasing diffusion weightings and, thus, the tissue signal finally reaches the noise level of the image (Fig. 5a), which will bias the determined ADCs if the noise level is not incorporated into the signal analysis<sup>71</sup>. As a consequence, an optimal diffusion weighting should balance between sufficient diffusion contrast and sufficient SNR. A frequently found rule of thumb is that the  $b$ -value should be about the inverse of the expected ADC<sup>32</sup>; e. g., for ADCs of  $1.0 \times 10^{-3} \text{ mm}^2/\text{s}$ , the  $b$ -value should be chosen around  $1000 \text{ s}/\text{mm}^2$ .

In DWI of the liver and particularly of the kidneys, generally lower  $b$ -values are applied than in neurological applications since the corresponding ADCs are considerably higher (cf. Table 1). Whereas typical ADCs in brain tissue range from 0.7 to  $0.9 \times 10^{-3} \text{ mm}^2/\text{s}$  and are assessed with diffusion

weightings of about  $1000 \text{ s}/\text{mm}^2$ , the ADCs of renal tissue ( $2.2$  to  $2.4 \times 10^{-3} \text{ mm}^2/\text{s}$ ) or of liver tissue ( $1.8 \times 10^{-3} \text{ mm}^2/\text{s}$ ) are considerably higher. Thus,  $b$ -values between  $300$  and  $600 \text{ s}/\text{mm}^2$  can be used for abdominal DWI. In addition to signal attenuations comparable to those in DWI of the brain, lower  $b$ -values have the advantage that shorter diffusion gradients can be used and, thus, shorter echo times become possible. This is particularly important in tissue with short T2 relaxation times (relative to T2 times in brain tissue) such as the liver or the kidneys<sup>72</sup>.

In DWI of normal and pathological bone marrow, a relatively large range of ADCs is observed (from about  $0.2$  to  $2.0 \times 10^{-3} \text{ mm}^2/\text{s}$ ); thus, it is difficult to define an optimal  $b$ -value. Since the SNR is generally very low in DWI of the bone marrow, the optimal diffusion weighting should be somewhat lower than for DWI of the brain. Frequently applied  $b$ -values are in the range of  $500$  to  $600 \text{ s}/\text{mm}^2$  for both echo-planar and fast-spin-echo measurements. To obtain a more acceptable image quality with EPI sequences, even lower optimal  $b$ -values of about  $300 \text{ s}/\text{mm}^2$  have been proposed<sup>73</sup>, although this may decrease the precision of the determined ADCs because of the low attenuation.

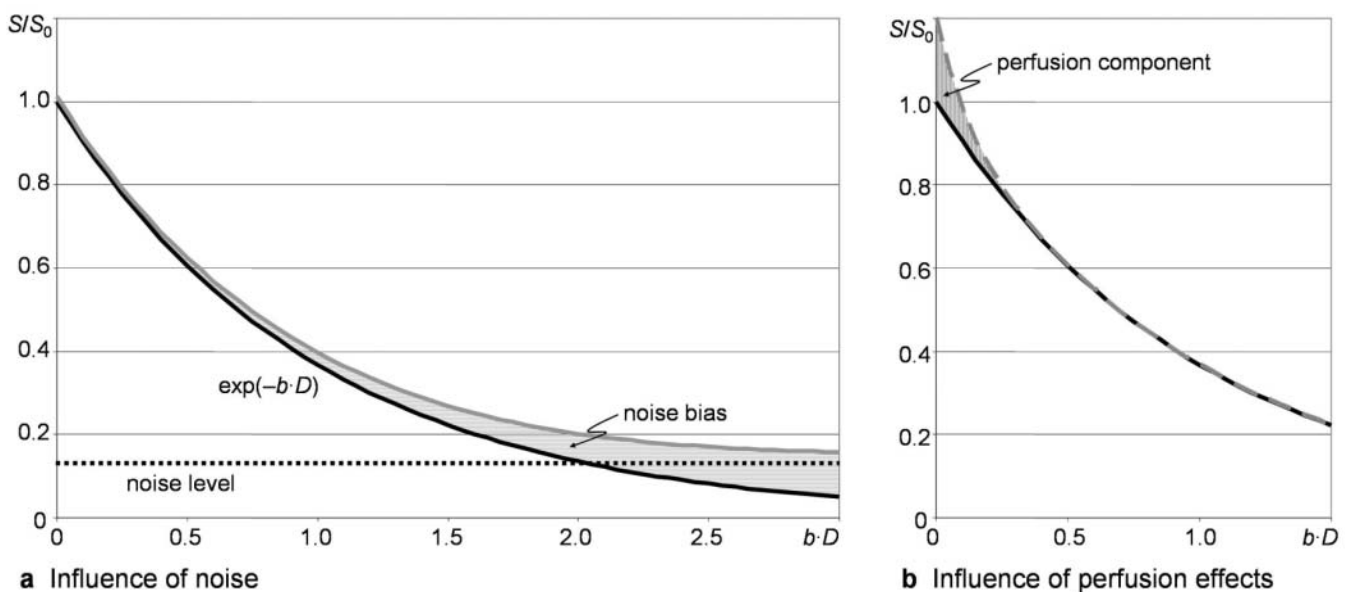


**Figure 5:** Signal attenuation,  $S/S_0$ , in DWI as a function of the diffusion weighting,  $b$ , for a given diffusion coefficient,  $D$ .  $S_0$  denotes the signal without diffusion weighting, without noise, and without additional perfusion component. (a) Signal attenuation without noise (black line) and with noise (gray line); the background noise level is indicated as dotted black line. With noise, the attenuated signal appears increased at high  $b$ -values. (b) Signal attenuation without perfusion effects (black line) and with perfusion effects (dashed gray line); the attenuated signal appears increased at low  $b$ -values.

In whole-body DWI, the “diffusion-weighted whole-body imaging with background body signal suppression” (DWIBS) approach is aimed to suppress the signal of most tissues while high-lighting potential malignancies or suspect lymph nodes in grayscale-inverted reformatted reconstructions. Therefore, relatively high diffusion weightings (and an excellent fat suppression) are required; typically, axial diffusion-weighted EPI sequences with a b-value of 1000 s/mm<sup>2</sup> are applied<sup>24, 25</sup>.

In addition to the maximum b-value, the optimal choice of the minimal b-value should be considered as well. At low b-values between 0 and about 100 s/mm<sup>2</sup>, diffusion-weighted techniques are sensitive not only to diffusion processes but also to capillary tissue perfusion<sup>74</sup>. The combined effect of both components results in a biexponential signal attenuation that is dominated by perfusion at low b-values and by diffusion at higher b-values (Fig. 5b)<sup>75, 76</sup>. Thus, either a biexponential analysis of the signal attenuation or a minimal b-value of about 50 to 100 s/mm<sup>2</sup> is recommended to reduce the influence of perfusion effects and to measure diffusion as the predominant attenuating effect.

## Conclusions

Diffusion-weighted imaging of the body is a promising tool for the detection and characterization of pathologies in various organs or tissues. It is, however, less robust than EPI-based DWI or DTI of the brain, and several improvements of the measurement techniques as well as specific optimizations of the imaging protocols are required to obtain reproducible results and acceptable image quality in body DWI. The most important alternative pulse sequence types employed for DWI outside the brain are single-shot and PROPELLER fast-spin-echo approaches as well as steady-state free-precession sequences. If these sequences are applied with adapted b-values (typically lower than in DWI of the brain), sufficient image quality can be obtained and the reliable quantification of diffusion parameters in the body is possible.

## Acknowledgements

This work was supported in parts by the Deutsche Forschungsgemeinschaft (DFG), grant no. DI 1413/1-1.

## References

1. Karaarslan E, Arslan A. Diffusion weighted MR imaging in non-infarct lesions of the brain. *Eur J Radiol* 2008;65(3):402–16.
2. Schaefer PW, Copen WA, Lev MH, et al. Diffusion-weighted imaging in acute stroke. *Magn Reson Imaging Clin N Am* 2006;14(2):141–68.
3. Brazzelli M, Sandercock PA, Chappell FM, et al. Magnetic resonance imaging versus computed tomography for detection of acute vascular lesions in patients presenting with stroke symptoms. *Cochrane Database Syst Rev* 2009;(4):CD007424.
4. Boulanger Y, Amara M, Lepanto L, et al. Diffusion-weighted MR imaging of the liver of hepatitis C patients. *NMR Biomed* 2003;16(3):132–6.
5. Parikh T, Drew SJ, Lee VS, et al. Focal liver lesion detection and characterization with diffusion-weighted MR imaging: comparison with standard breath-hold T2-weighted imaging. *Radiology* 2008;246(3):812–22.
6. Zech CJ, Herrmann KA, Dietrich O, et al. Black-blood diffusion-weighted EPI acquisition of the liver with parallel imaging: comparison with a standard T2-weighted sequence for detection of focal liver lesions. *Invest Radiol* 2008;43(4):261–6.
7. Zhang J, Tehrani YM, Wang L, et al. Renal masses: characterization with diffusion-weighted MR imaging—a preliminary experience. *Radiology* 2008;247(2):458–64.
8. Notohamiprodjo M, Glaser C, Herrmann KA, et al. Diffusion tensor imaging of the kidney with parallel imaging: initial clinical experience. *Invest Radiol* 2008;43(10):677–85.
9. Taouli B, Thakur RK, Mannelli L, et al. Renal lesions: characterization with diffusion-weighted imaging versus contrast-enhanced MR imaging. *Radiology* 2009;251(2):398–407.
10. Sinha S, Lucas-Quesada FA, Sinha U, et al. In vivo diffusion-weighted MRI of the breast: potential for lesion characterization. *J Magn Reson Imaging* 2002;15(6):693–704.
11. Tsushima Y, Takahashi-Taketomi A, Endo K. Magnetic resonance (MR) differential diagnosis of breast tumors using apparent diffusion coefficient (ADC) on 1.5-T. *J Magn Reson Imaging* 2009;30(2):249–55.
12. Bogner W, Gruber S, Pinker K, et al. Diffusion-weighted MR for differentiation of breast lesions at 3.0 T: how does selection of diffusion protocols affect diagnosis? *Radiology* 2009;253(2):341–51.
13. Yabuuchi H, Matsuo Y, Kamitani T, et al. Non-mass-like enhancement on contrast-enhanced breast MR imaging: Lesion characterization using combination of dynamic contrast-enhanced and diffusion-weighted MR images. *Eur J Radiol* 2009; [epub ahead of print].
14. Sinha S, Sinha U. In vivo diffusion tensor imaging of the human prostate. *Magn Reson Med* 2004;52(3):530–7.
15. Mazaheri Y, Shukla-Dave A, Hricak H, et al. Prostate cancer: identification with combined diffusion-weighted MR imaging and 3D 1H MR spectroscopic imaging—correlation with pathologic findings. *Radiology* 2008;246(2):480–8.

16. Jacobs MA, Ouwerkerk R, Petrowski K, et al. Diffusion-weighted imaging with apparent diffusion coefficient mapping and spectroscopy in prostate cancer. *Top Magn Reson Imaging* 2008;19(6):261–72.
17. Holzapfel K, Duetsch S, Fauser C, et al. Value of diffusion-weighted MR imaging in the differentiation between benign and malignant cervical lymph nodes. *Eur J Radiol* 2009;72(3):381–7.
18. Klerkx WM, Mali WM, Peter Heintz A, et al. Observer variation of magnetic resonance imaging and diffusion weighted imaging in pelvic lymph node detection. *Eur J Radiol* 2009; [epub ahead of print].
19. Dietrich O, Raya JG, Sommer J, et al. A comparative evaluation of a RARE-based single-shot pulse sequence for diffusion-weighted MRI of musculoskeletal soft-tissue tumors. *Eur Radiol* 2005;15(4):772–83.
20. Nagata S, Nishimura H, Uchida M, et al. Diffusion-weighted imaging of soft tissue tumors: usefulness of the apparent diffusion coefficient for differential diagnosis. *Radiat Med* 2008;26(5):287–95.
21. Baur A, Stäbler A, Brüning R, et al. Diffusion-weighted MR imaging of bone marrow: differentiation of benign versus pathologic compression fractures. *Radiology* 1998;207(2):349–56.
22. Raya JG, Dietrich O, Reiser MF, et al. Methods and applications of diffusion imaging of vertebral bone marrow. *J Magn Reson Imaging* 2006;24(6):1207–20.
23. Dietrich O, Biffar A, Reiser MF, et al. Diffusion-weighted imaging of bone marrow. *Semin Musculoskelet Radiol* 2009;13(2):134–44.
24. Takahara T, Imai Y, Yamashita T, et al. Diffusion weighted whole body imaging with background body signal suppression (DWIBS): technical improvement using free breathing, STIR and high resolution 3D display. *Radiat Med* 2004;22(4):275–82.
25. Kwee TC, Takahara T, Ochiai R, et al. Whole-body diffusion-weighted magnetic resonance imaging. *Eur J Radiol* 2009;70(3):409–17.
26. Raya JG, Dietrich O, Reiser MF, et al. Techniques for diffusion-weighted imaging of bone marrow. *Eur J Radiol* 2005;55(1):64–73.
27. Koh DM, Takahara T, Imai Y, et al. Practical aspects of assessing tumors using clinical diffusion-weighted imaging in the body. *Magn Reson Med Sci* 2007;6(4):211–24.
28. Dietrich O, Reiser MF, Schoenberg SO. Artifacts in 3-T MRI: physical background and reduction strategies. *Eur J Radiol* 2008;65(1):29–35.
29. Dietrich O. Diffusion-weighted imaging and diffusion tensor imaging. In: Reiser MF, Semmler W, Hricak H, editors. *Magnetic resonance tomography*. Berlin Heidelberg New York: Springer, 2008: 130–52.
30. Hahn EL. Spin echoes. *Phys Rev* 1950;80(4):580–94.
31. Stejskal EO, Tanner JE. Spin diffusion measurements: spin echoes in the presence of a time-dependent field gradient. *J Chem Phys* 1965;42(1):288–92.
32. Xing D, Papadakis NG, Huang CL, et al. Optimised diffusion-weighting for measurement of apparent diffusion coefficient (ADC) in human brain. *Magn Reson Imaging* 1997;15(7):771–84.
33. Trouard TP, Sabharwal Y, Altbach MI, et al. Analysis and comparison of motion-correction techniques in diffusion-weighted imaging. *J Magn Reson Imaging* 1996;6(6):925–35.
34. Norris DG. Implications of bulk motion for diffusion-weighted imaging experiments: effects, mechanisms, and solutions. *J Magn Reson Imaging* 2001;13(4):486–95.
35. Le Bihan D, Poupon C, Amadon A, et al. Artifacts and pitfalls in diffusion MRI. *J Magn Reson Imaging* 2006;24(3):478–88.
36. Basser PJ, Mattiello J, LeBihan D. MR diffusion tensor spectroscopy and imaging. *Biophys J* 1994;66(1):259–67.
37. Basser PJ, Pierpaoli C. Microstructural and physiological features of tissues elucidated by quantitative-diffusion-tensor MRI. *J Magn Reson B* 1996;111(3):209–19.
38. Basser PJ, Pierpaoli C. A simplified method to measure the diffusion tensor from seven MR images. *Magn Reson Med* 1998;39(6):928–34.
39. Mukherjee P, Berman JI, Chung SW, et al. Diffusion tensor MR imaging and fiber tractography: theoretic underpinnings. *AJNR Am J Neuroradiol* 2008;29(4):632–41.
40. Merboldt KD, Hänicke W, Frahm J. Self-diffusion NMR imaging using stimulated echoes. *J Magn Reson* 1985;64(3):479–86.
41. Taylor DG, Bushell MC. The spatial mapping of translational diffusion coefficients by the NMR imaging technique. *Phys Med Biol* 1985;30(4):345–9.
42. Le Bihan D, Breton E, Lallemand D, et al. MR imaging of intravoxel incoherent motions: application to diffusion and perfusion in neurologic disorders. *Radiology* 1986;161(2):401–7.
43. Ordidge RJ, Helpert JA, Qing ZX, et al. Correction of motional artifacts in diffusion-weighted MR images using navigator echoes. *Magn Reson Imaging* 1994;12(3):455–60.
44. Anderson AW, Gore JC. Analysis and correction of motion artifacts in diffusion weighted imaging. *Magn Reson Med* 1994;32(3):379–87.
45. Dietrich O, Heiland S, Benner T, et al. Reducing motion artifacts in diffusion-weighted MRI of the brain: efficacy of navigator echo correction and pulse triggering. *Neuroradiology* 2000;42(2):85–91.
46. Gmitro AF, Alexander AL. Use of a projection reconstruction method to decrease motion sensitivity in diffusion-weighted MRI. *Magn Reson Med* 1993;29(6):835–8.
47. Dietrich O, Herlihy A, Dannels WR, et al. Diffusion-weighted imaging of the spine using radial k-space trajectories. *MAGMA Magn Reson Mater Phy* 2001;12(1):23–31.
48. Gudbjartsson H, Maier SE, Mulkern RV, et al. Line scan diffusion imaging. *Magn Reson Med* 1996;36(4):509–19.
49. Turner R, Le Bihan D, Maier J, et al. Echo-planar imaging of intravoxel incoherent motion. *Radiology* 1990;177(2):407–14.
50. Brockstedt S, Moore JR, Thomsen C, et al. High-resolution diffusion imaging using phase-corrected segmented echo-planar imaging. *Magn Reson Imaging* 2000;18(6):649–57.
51. Schoenberg SO, Dietrich O, Reiser MF. *Parallel imaging in clinical MR applications*. Berlin Heidelberg New York: Springer, 2007.
52. Pruessmann KP, Weiger M, Scheidegger MB, et al. SENSE: sensitivity encoding for fast MRI. *Magn Reson Med* 1999;42(5):952–62.
53. Griswold MA, Jakob PM, Heidemann RM, et al. Generalized autocalibrating partially parallel acquisitions (GRAPPA). *Magn Reson Med* 2002;47(6):1202–10.
54. Jaermann T, Pruessmann KP, Valavanis A, et al. Influence of SENSE on image properties in high-resolution single-shot echo-planar DTI. *Magn Reson Med* 2006;55(2):335–42.
55. Norris DG, Börnert P, Reese T, et al. On the application of ultrafast RARE experiments. *Magn Reson Med* 1992;27(1):142–64.

56. Lövblad KO, Jakob PM, Chen Q, et al. Turbo spin-echo diffusion-weighted MR of ischemic stroke. *AJNR Am J Neuroradiol* 1998;19(2):201–8.
57. Schick F. SPLICE: sub-second diffusion-sensitive MR imaging using a modified fast spin-echo acquisition mode. *Magn Reson Med* 1997;38(4):638–44.
58. Alsop DC. Phase insensitive preparation of single-shot RARE: application to diffusion imaging in humans. *Magn Reson Med* 1997;38(4):527–33.
59. Le Roux P. Non-CPMG Fast Spin Echo with full signal. *J Magn Reson* 2002;155(2):278–92.
60. Norris DG. Selective parity RARE imaging. *Magn Reson Med* 2007;58(4):643–9. (Erratum in: *Magn Reson Med* 2008;59(2):440.)
61. Pipe JG, Farthing VG, Forbes KP. Multishot diffusion-weighted FSE using PROPELLER MRI. *Magn Reson Med* 2002;47(1):42–52. (Erratum in: *Magn Reson Med* 2002;47(3):621.)
62. Deng J, Miller FH, Salem R, et al. Multishot diffusion-weighted PROPELLER magnetic resonance imaging of the abdomen. *Invest Radiol* 2006;41(10):769–75.
63. Gyngell ML. The application of steady-state free precession in rapid 2DFT NMR imaging: FAST and CE-FAST sequences. *Magn Reson Imaging* 1988;6(4):415–9.
64. Bruder H, Fischer H, Graumann R, et al. A new steady-state imaging sequence for simultaneous acquisition of two MR images with clearly different contrasts. *Magn Reson Med* 1988;7(1):35–42.
65. Le Bihan D. Intravoxel incoherent motion imaging using steady-state free precession. *Magn Reson Med* 1988;7(3):346–51.
66. Merboldt KD, Bruhn H, Frahm J, et al. MRI of "diffusion" in the human brain: new results using a modified CE-FAST sequence. *Magn Reson Med* 1989;9(3):423–9.
67. Kaiser R, Bartholdi E, Ernst RR. Diffusion and field-gradient effects in NMR Fourier spectroscopy. *J Chem Phys* 1974;60(8):2966–79.
68. Wu EX, Buxton RB. Effect of diffusion on the steady-state magnetization with pulsed field gradients. *J Magn Reson* 1990;90(2):243–53.
69. Miller KL, Hargreaves BA, Gold GE, et al. Steady-state diffusion-weighted imaging of in vivo knee cartilage. *Magn Reson Med* 2004;51(2):394–8.
70. Sakamoto J, Yoshino N, Okochi K, et al. Tissue characterization of head and neck lesions using diffusion-weighted MR imaging with SPLICE. *Eur J Radiol* 2009;69(2):260–8.
71. Dietrich O, Heiland S, Sartor K. Noise correction for the exact determination of apparent diffusion coefficients at low SNR. *Magn Reson Med* 2001;45(3):448–53.
72. Stanisz GJ, Odobina EE, Pun J, et al. T1, T2 relaxation and magnetization transfer in tissue at 3T. *Magn Reson Med* 2005;54(3):507–12.
73. Tang G, Liu Y, Li W, et al. Optimization of b value in diffusion-weighted MRI for the differential diagnosis of benign and malignant vertebral fractures. *Skeletal Radiol* 2007;36(11):1035–41.
74. Le Bihan D, Breton E, Lallemand D, et al. Separation of diffusion and perfusion in intravoxel incoherent motion MR imaging. *Radiology* 1988;168(2):497–505.
75. van Rijswijk CS, Kunz P, Hogendoorn PC, et al. Diffusion-weighted MRI in the characterization of soft-tissue tumors. *J Magn Reson Imaging* 2002;15(3):302–7.
76. Yeung DK, Wong SY, Griffith JF, et al. Bone marrow diffusion in osteoporosis: evaluation with quantitative MR diffusion imaging. *J Magn Reson Imaging* 2004;19(2):222–8.
77. Tofts PS, Lloyd D, Clark CA, et al. Test liquids for quantitative MRI measurements of self-diffusion coefficient in vivo. *Magn Reson Med* 2000;43(3):368–74.
78. Mills R. Self-diffusion in normal and heavy water in the range 1–45°. *J Phys Chem* 1973;77(5):685–8.
79. Helenius J, Soinne L, Perkio J, et al. Diffusion-weighted MR imaging in normal human brains in various age groups. *AJNR Am J Neuroradiol* 2002;23(2):194–9.